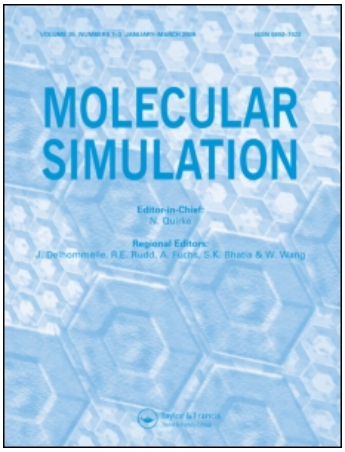

Molecular Simulation
Publication details, including instructions for authors and subscription information:
http://www.informaworld.com/smpp/title~content=t713644482

Structural Phase Transition of Di-Block Polyampholyte

H. Shimizu[ab]; K. Uehara[c]; K. Yamamoto[a]; Y. Hiwatari[a]
[a] Department of Computational Science, Faculty of Science, Kanazawa University, Kanazawa, Japan [b] Department of Physics, Faculty of Science, Shinshu University, Matsumoto, Japan [c] Steacie Institute for Molecular Sciences, National Research Council, Canada, Ottawa, Ontario, Canada

To cite this Article Shimizu, H. , Uehara, K. , Yamamoto, K. and Hiwatari, Y.(1999) 'Structural Phase Transition of Di-Block Polyampholyte', Molecular Simulation, 22: 4, 285 — 301
To link to this Article: DOI: 10.1080/08927029908022102
URL: http://dx.doi.org/10.1080/08927029908022102

Molecular Simulation, 1999, Vol. 22, pp. 285–301
Reprints available directly from the publisher
Photocopying permitted by license only

STRUCTURAL PHASE TRANSITION OF DI-BLOCK POLYAMPHOLYTE

H. SHIMIZU [a,*], K. UEHARA [b], K. YAMAMOTO [a] and Y. HIWATARI [a,†]

[a]*Department of Computational Science, Faculty of Science, Kanazawa University, Kakuma, Kanazawa, 920-1192, Japan;*
[b]*Steacie Institute for Molecular Sciences, National Research Council, Canada, Ottawa, Ontario, K1A 0R6, Canada*

(Received December 1998; accepted February 1999)

We have performed both conventional canonical molecular dynamics (MD) and multicanonical MD (MMD) simulations for a single di-block polyampholyte in vacuum to investigate possible structural phase transitions. The conventional canonical MD simulation for temperature $T^* > 0.05$ gives reliable results, since these are independent of the initial conformation. The MMD simulation results for temperature $T^* > 0.05$ are in good agreement with those of the conventional canonical MD simulation. Glassy-like states are obtained when quenched into temperatures below $T^* \sim 0.05$ with a straight chain structure as an initial conformation. On the other hand a spherical double helical structure is obtained when the temperature is gradually lowered to $T^* \sim 0.01$. Also we find a stretched double helical structure at $T^* \sim 0.01$ which changes to the spherical double helical structure by annealing and quenching.

Keywords: Molecular dynamics simulation; multicanonical algorithm; constraint dynamics; charged polymer; Coulomb interaction; structural transition

1. INTRODUCTION

It has long been discussed that the structural conformation of proteins is determined by the sequence of amino acid [1] and there exists a certain pathway for the folding of proteins [2]. These discussions are based on

*Present address: Department of Physics, Faculty of Science, Shinshu University, 3-1-1 Asahi, Matsumoto, 390-8621, Japan.
†Corresponding author.

experimental results. Molecular dynamics (MD) and Monte Carlo simulations for a variety of model of polymers have widely been performed to obtain theoretical supports for these hypotheses. Most of models of polymers which have been used so far assume only electrically neutral monomers. However many proteins contain both electrically neutral and electrically charged amino acids. Experimentally Minor and Kim [3] have showed that long range interactions play important roles on folding of proteins. Thus it is expected that Coulomb interactions are important parts of interactions in folding of proteins. A polymer which contains both positively and negatively charged monomers in a chain is called polyampholyte (PA). There are some theoretical works on PA [4–8]. The sequence of charges is generally assumed to be random, while an alternative sequence of charges is assumed in Ref. [8]. The scaling relation between the gyration radius and the temperature are investigated in Refs. [4–8] and the dependency of gyration radius on the total charge has been investigated in Ref. [8]. In this paper we investigate the structural transition of PA with a simple sequence of charges in 3 dimensional space by applying both the conventional canonical MD and the multicanonical MD (MMD) methods.

In Section 2 the model considered in this paper is presented. The details of the MD and the MMD simulations are given in Section 3. The results of MD simulations are shown in Section 4. Finally Section 5 is devoted for the discussion and conclusion.

2. MODEL

As mentioned in Section 1, long range interactions such as Coulomb interactions are considered to be important in folding of proteins. PA is one of such model polymers as it consists of positively and negatively charged monomers on a chain. PA has at least two characteristic features in general resemblance with real proteins as it is a hetero polymer and coulombic system. It presents an enormous different kinds of polymers according to the magnitude of charges to each monomers as well as the sequence of monomers. In real proteins the magnitude of charges to each amino acids and the sequence of them are different for each protein. In this paper in order to get insights into the effect of the charge sequence on folding of PA, we consider a model polymer which contains the same numbers of positively and negatively charged monomers and $N/2$ monomers among N total monomers are positively charged on one side of the chain and the remaining $N/2$ monomers are negatively charged on another side. We call this model

polymer *di-block PA* hereafter. We consider only one di-block PA in vacuum. We take the potential functions for this polymer as follows:

$$E = \sum_{i=1}^{N} \sum_{j=i+2}^{N} \left\{ \frac{q_i q_j}{r_{ij}} + 4\zeta \left(\frac{\sigma}{r_{ij}} \right)^{12} \right\} \tag{1}$$

$$r_{ij} = |\mathbf{x}_i - \mathbf{x}_j|,$$

where q_i is the charge on each monomer. $q_i = e$ for $i = 1 \sim N/2$ and $q_i = -e$ for $i = N/2 + 1 \sim N$, where e is the elementary electric charge ($e > 0$). The first term of Eq. (1) represents the Coulomb interaction and the second term is the soft core interaction for the excluded volume so as to prevent intersection of bonds. Due to the bond length constraint which will be described in detail in Section 3.2 the energy contribution from the bonding monomers becomes constant. Hence we neglect these constant in Eq. (1) and therefore the summation over j is taken from $i+2$ to N. The parameters which we have used in this paper are shown in Table I. A schematic illustration of di-block PA is shown in Figure 1. Throughout this paper we use the reduced temperature T^* which is related to the real temperature (T) through

$$T^* \equiv \left(\frac{e^2}{r_0 k_B T} \right)^{-1}, \tag{2}$$

where e is the elementary electric charge, k_B is Boltzmann constant and r_0 is the length of the monomer bonds, being kept constant during the simulation. In this paper the number of monomer (N) is 60.

3. SIMULATION METHOD

3.1. MD Calculations

In polymers the conventional canonical MD simulation have been widely used to investigate physical properties. But it has been known that the

TABLE I Parameters for the potential function. "e" is the elementary electric charge ($e > 0$). "r_0" is the distance of neighboring monomers. "m" is the mass of monomer

q_i	e ($i = 1 \sim N/2$)
	$-e$ ($i = N/2 + 1 \sim N$)
r_0	1.80 [Å]
ζ	1.09×10^{-20} [J]
σ	1.80 [Å]
m	2.29×10^{-25} [kg]

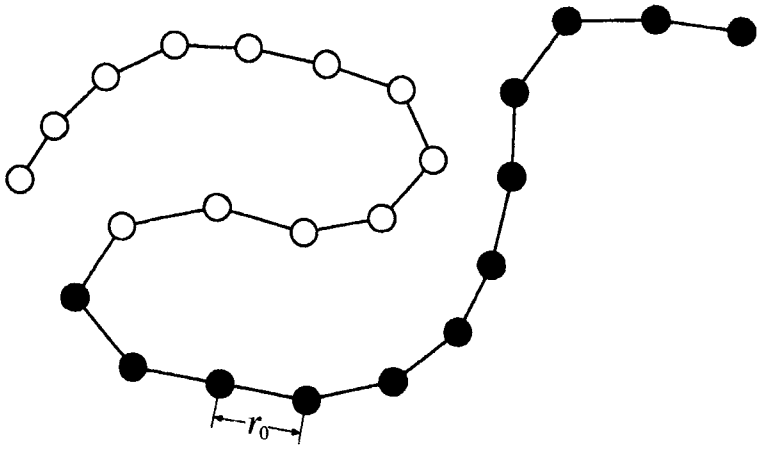

FIGURE 1 Schematic illustration of di-block PA. "r_0" is the bond length of the neighboring monomers. White and black circles represent the positively and negatively charged monomer, respectively.

conventional canonical MD simulation sometimes can not produce reliable statistical ensemble because complexities of potential functions of such systems prevent from sampling over a wide area of the phase space. For this point it is highly desired to improve the canonical MD simulation method. Berg and Neuhaus [9] have firstly proposed the multicanonical algorithm and applied it to a Monte Carlo sampling. This algorithm has been developed to the MD simulation by Nakajima *et al.* [10]. The model which we consider in this paper (Eq. (1)) is very simple, but still enough complex in the sense that it builds statistically large numbers of local minima of energy states. Therefore it must be a good model to study by numerical simulations with both the conventional canonical MD and MMD methods. We have used the constraint method of temperature [11, 12] and the NIMM (Non-Iterative Matrix Method) [13 – 15] for the bond length constraint between the nearest monomer distance. We used the velocity Verlet method [16] to integrate the equation of motion. The time step is chosen to be ~ 0.5 fs and the number of step for one conventional canonical MD and MMD simulation is 4×10^7 steps after a preliminary sampling over several 10^5 steps. The initial velocity of all monomers was determined randomly.

3.2. MMD Method with the Bond Length Constraint

The basic procedure of the MMD simulation used in this paper is the same as in Ref. [10] but with a different way of estimates for the logarithmic

derivative of the probability distribution. Below the simulation procedure is described in detail.

The concept of the MMD method is to produce the probability distribution $\mathcal{P}(E)$ independent of the energy of the system.

$$\mathcal{P}(E) = \frac{1}{\mathcal{Z}} n(E) \exp(-W(E)) = \text{constant}, \tag{3}$$
$$\mathcal{Z} = \sum_E n(E) \exp(-W(E)),$$

where E is the total energy of the system, $n(E)$ is the density of states and $\mathcal{Z}$ is the partition function. Equation (3) means that during a simulation the system can take a wide area of the phase space without potential energy barriers. From Eq. (3) one can find that $W(E)$ is related to the density of states as

$$W(E) = \log n(E) \tag{4}$$

except for a factor independent of E. This $W(E)$ is just what we want to evaluate from the MD simulation. First we assume the functional form of $W(E)$ like

$$W(E) = \frac{\mathcal{E}(E)}{k_B T_0}, \tag{5}$$

where T_0 is a constant with units of temperature. Then Eq. (3) is rewritten as

$$\mathcal{P}_{T_0}(E) \propto \exp\left(-\frac{\mathcal{E}(E)}{k_B T_0}\right) \tag{6}$$

This equation can be regarded as the canonical probability distribution for the system of which the energy is $\mathcal{E}(E)$ and the temperature is T_0. We still do not know $W(E)$ (or $\mathcal{E}(E)$). We initially approximate $\mathcal{E}(E)$ by substituting the density of states evaluated from the result of conventional canonical MD simulation in Eq. (4)

$$\begin{aligned} \mathcal{E}(E) &= k_B T_0 \log n_c(E) \\ &= E + k_B T_0 \log P_{T_0}(E) \\ n_c(E) &= Z_{T_0} P_{T_0}(E) \exp\left(\frac{E}{k_B T_0}\right). \end{aligned} \tag{7}$$

In Eq. (7) we eliminate the term "$k_B T_0 \log Z_{T_0}$" because it is independent of E. According to Eq. (7), the force on monomer i is modified as

$$\begin{aligned}\mathcal{F}_i(t) &= -\nabla_i \mathcal{E}(E) \\ &= -\frac{d\mathcal{E}(E)}{dE}\nabla_i E \\ &= -\left(1 + k_B T_0 \frac{d}{dE}\log P_{T_0}(E)\right)\nabla_i E. \end{aligned} \tag{8}$$

If the second term in Eq. (8) is neglected, $\mathcal{F}_i(t)$ becomes to the force for the conventional canonical MD. Now standard MMD simulation [10] uses the force which further modifies Eq. (8) so as to keep the temperature constant by adding an extra term "$-\alpha(t)\mathbf{p}_i(t)$". In our simulation another external force ($\mathbf{F}_i^{\text{ext}}(t)$) comes from the constraint of monomers' bond length is also added. Therefore the equations of motion become

$$\dot{\mathbf{x}}_i(t) = \frac{\mathbf{p}_i(t)}{m_i}, \tag{9}$$

$$\dot{\mathbf{p}}_i(t) = \mathcal{F}_i(t) - \alpha(t)\mathbf{p}_i(t) + \mathbf{F}_i^{\text{ext}}(t). \tag{10}$$

We perform the canonical MD simulation with these equation of motions at temperature T_0. As described in Section 3.1, we use the constraint method [11, 12] to keep the temperature constant. So the kinetic energy is kept constant during the simulation and E and $\mathcal{E}(E)$ in Eq. (8) are regarded as the potential energy. $\mathbf{F}_i^{\text{ext}}(t)$ and $\alpha(t)$ in Eq. (10) must be simultaneously determined. However if we expand the NIMM to take into consideration the temperature constraint, the convenience of the NIMM is lost. Thus we firstly calculate $\mathcal{F}_i(t)$, next $\mathbf{F}_i^{\text{ext}}(t)$ and finally $\alpha(t)$ so as the combined forces "$\mathcal{F}_i(t) + \mathbf{F}_i^{\text{ext}}(t)$" to keep the temperature constant. The bond length constraint is corrupted with this procedure, but the error is evaluated as

$$\frac{\langle \Delta r \rangle}{r_0} \equiv \sqrt{\frac{1}{NN_{\text{step}}}\sum_{n=1}^{N_{\text{step}}}\sum_{i=1}^{N-1}(r_{ii+1}(t_n) - r_0)^2}\Big/ r_0, \tag{11}$$

which is less than 1×10^{-4}. In Eq. (11) r_0 is the bond length between connected monomers, N the number of monomers and N_{step} the number of steps for each MD simulation. By performing a canonical MD simulation with the equation of motions, Eqs. (9) and (10), a new probability distribution is obtained. If this probability distribution satisfies Eq. (3) within the

energy region of our interest, we go to the next step, *reweightting procedure*. But if the condition is not satisfied, we approximate the density of states as

$$n_{\mathrm{mc}}(E) = \mathcal{Z}_{T_0}\mathcal{P}_{T_0}(E)\exp\left(\frac{\mathcal{E}(E)}{k_B T_0}\right), \tag{12}$$

then substitute it in Eq. (4) to estimate new $\mathcal{E}(E)$ as

$$\mathcal{E}_{\mathrm{new}}(E) = \mathcal{E}_{\mathrm{old}}(E) + k_B T_0 \log \mathcal{P}_{T_0}(E), \tag{13}$$

and perform another canonical MD simulation until Eq. (3) becomes satisfied. Then we can evaluate the canonical probability distribution at an arbitrary temperature T with the *reweightting procedure*

$$P_T(E) \propto \mathcal{P}_{T_0}(E)\exp\left(\frac{\mathcal{E}(E)}{k_B T_0} - \frac{E}{k_B T}\right). \tag{14}$$

The procedure of MMD simulation is almost the same as the conventional canonical MD simulation. It is the force that MMD simulation is different from the conventional canonical MD simulation. In Eq. (8) the logarithmic derivative of the probability distribution is needed. An important point in this procedure is how to estimate the logarithmic derivative because, for instance, too large value of the logarithmic derivative corrupts the simulation easily. Then we estimate the probability distribution ($\mathcal{P}_{T_0}(E)$) as a sum of the Lorentzian

$$\mathcal{P}_{T_0}(E_m) = \frac{1}{N_{\mathrm{step}}}\sum_{n=1}^{N_E}\mathcal{H}_{T_0}(E_n)\frac{1}{2\pi\delta E}\frac{1}{1+\left(\frac{E_m - E_n}{\delta E}\right)^2}, \tag{15}$$

$$N_{\mathrm{step}} = \sum_{m=1}^{N_E}\mathcal{H}_{T_0}(E_m), \tag{16}$$

where $\mathcal{H}_{T_0}(E_m)$, E_m and δE are the energy histogram, the energy at m-th step and the energy interval which is used to obtain the energy histogram, respectively. The energy histogram is sampled within the energy region expressed by $E_n = E_0 + (n-1)\delta E$, ($n = 1 \sim N_E$). For the arbitrary value of energy E we calculate the $\mathcal{P}_{T_0}(E)$ and its energy derivative with the cubic spline method. Then the $\mathcal{P}_{T_0}(E)$ results in exhibiting a smooth tail in either the high or low energy region. Furthermore we can obtain an analytical

functional form for the logarithmic derivative of the probability distribution so that we do not need fitting the probability distribution.

4. RESULTS

Figure 2 shows the probability distribution ($P(\varepsilon)$) obtained by the conventional canonical MD at $T^* \sim 0.03, 0.108, 0.32$ and that of the MMD after 19 times iterations at $T^* \sim 0.108$. The initial conformation of the di-block PA was started from a straight chain. The $P(\varepsilon)$ of the MMD in this figure has a flat in the energy region $\varepsilon = -1.55 \sim -1.1$, which covers that of conventional canonical MD at $T^* \sim 0.03$ to 0.32. Hence we expect the $P(\varepsilon)$ reweighted to the result of MMD simulation is reliable over the temperature region $T^* = 0.03 \sim 0.32$ and should be compared with that obtained by the conventional canonical MD. Figure 3 is the $P(\varepsilon)$ of the conventional canonical MD and the $P(\varepsilon)$ obtained through the MMD simulation and reweighted to the temperature $T^* \sim 0.108$. Both are very similar to each other. We will show later that the conventional canonical MD simulation starting with some different initial conformations at $T^* \sim 0.05$ exhibits a

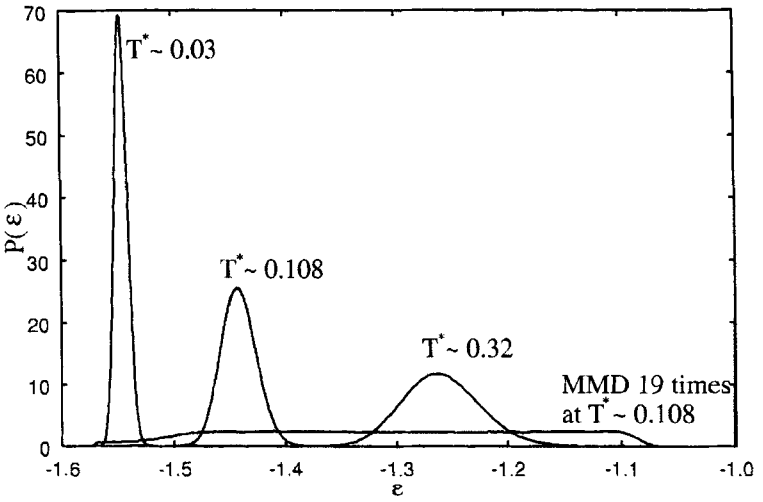

FIGURE 2 The probability distribution calculated by conventional canonical MD at $T^* \sim 0.03, 0.108, 0.32$ and by the MMD. The MMD simulation is iterated over 19 times at $T^* \sim 0.108$. "ε" is the reduced energy per monomer ($\varepsilon = (E/N)/(e^2/r_0)$).

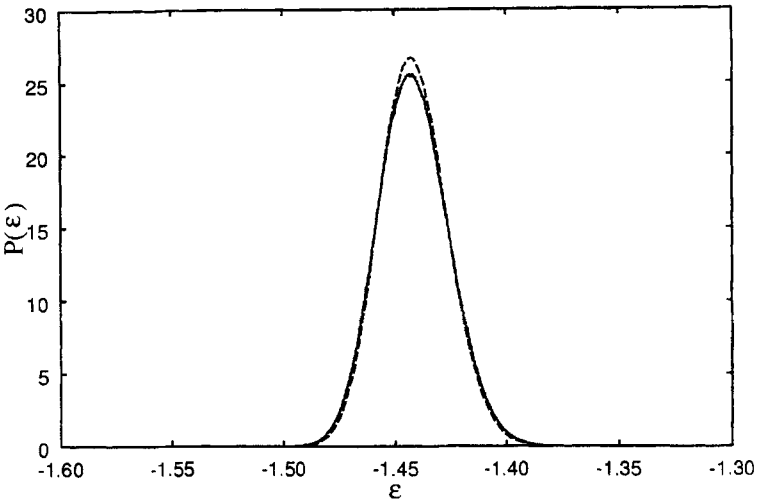

FIGURE 3 The probability distribution at $T^* \sim 0.108$. The solid line is the result of the conventional canonical MD and the broken line is obtained by reweightting the result of MMD. "ε" is the reduced energy per monomer ($\varepsilon = (E/N)/(e^2/r_0)$).

similar result. Therefore it turns out that this system must be free from being trapped into any locally minimum state if the temperature is higher than $T^* \sim 0.05$. Figures 4(a) and (b) show the average energy per one monomer and the specific heat, respectively. In these figures the circles indicate the results of the MMD simulation. The average energy obtained from the conventional canonical MD and MMD agree very well over the temperature region $T^* = 0.03 \sim 1.08$. There is a slight discrepancy between the specific heats in the low temperature region ($T^* = 0.03 \sim 0.108$), though there is a similar tendency to show a peak in both results. The MMD simulation is a better way of sampling at low temperatures to improve the conventional canonical MD simulation method.

Next we investigate the structure of the di-block PA in temperature region $T^* = 0.01 \sim 0.05$ in detail where a peak is found around $T^* \sim 0.02$ in the result of conventional canonical MD simulations (see Fig. 4(b)). As mentioned above, the initial conformation of di-block PA for the conventional canonical MD in Figures 4(a) and (b) was chosen a straight chain. It may be possible that the system was trapped into a certain glass state when the temperature is significantly low. Hence we have performed a number of other different series of simulations (Simulations II $\sim$ IV) in addition to the above simulation (Simulation I).

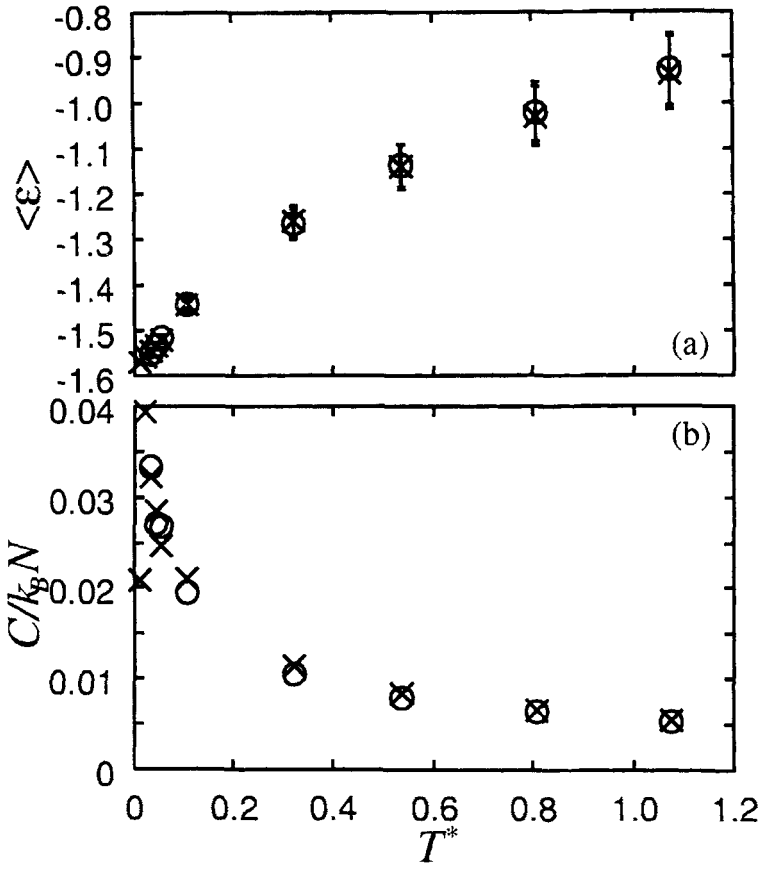

FIGURE 4 The temperature dependence of (a): potential energy and (b): specific heat. In both figures "○" is the result of the MMD simulation and "×" is the result of the conventional canonical MD simulations. $\langle\varepsilon\rangle = (\langle E\rangle/N)/(\epsilon^2/r_0)$, where $\langle E\rangle$ is the statistical average of the potential energy (see Eq. (1)).

4.1. Simulation II

1. a canonical MD simulation at $T^* \sim 0.05$ started with a straight chain structure. (II-1)
2. a canonical MD simulation at $T^* \sim 0.04$ started with the lowest energy conformation found in the simulation II-1. (II-2)
3. a canonical MD simulation at $T^* \sim 0.03$ started with the lowest energy conformation found in the simulation II-2. (II-3)
4. a canonical MD simulation at $T^* \sim 0.02$ started with the lowest energy conformation found in the simulation II-3. (II-4)
5. a canonical MD simulation at $T^* \sim 0.01$ started with the lowest energy conformation found in the simulation II-4. (II-5)

4.2. Simulation III

1. a canonical MD simulation at $T^* \sim 0.01$ started with a low energy conformation (Fig. 7(a)) found in the MMD simulation. (III-1)
2. a canonical MD simulation at $T^* \sim 0.02$ started with the lowest energy conformation found in the simulation III-1. (III-2)
3. a canonical MD simulation at $T^* \sim 0.03$ started with the lowest energy conformation found in the simulation III-2. (III-3)
4. a canonical MD simulation at $T^* \sim 0.04$ started with the lowest energy conformation found in the simulation III-3. (III-4)
5. a canonical MD simulation at $T^* \sim 0.05$ started with the lowest energy conformation found in the simulation III-4. (III-5)

4.3. Simulation IV

$1 \sim 3$. the same as the simulation III-1 through simulation III-3.

4. a canonical MD simulation at $T^* \sim 0.02$ started with the lowest energy conformation found in the simulation III-3. (IV-4)
5. a canonical MD simulation at $T^* \sim 0.01$ started with the lowest energy conformation found in the simulation IV-4. (IV-5)

The number of steps for every simulation is 4×10^7 after a preliminary sampling of over several 10^5 steps. The dependence of the energy, specific heat, gyration radius and hairpin parameter on the temperature for Simulations $I \sim IV$ are shown in Figure 5. The definition of gyration radius (R_g) and hairpin parameter (R_h) are

$$R_g \equiv \sqrt{\frac{1}{N}\sum_{i=1}^{N} \mathbf{x}_i^2 - \left(\frac{1}{N}\sum_{i=1}^{N} \mathbf{x}_i\right)^2} \Big/ R_{g0} \tag{17}$$

and

$$R_h \equiv \sqrt{\frac{1}{N/2}\sum_{i=1}^{N/2} (\mathbf{x}_i - \mathbf{x}_{N-i+1})^2} \Big/ R_{h0}, \tag{18}$$

where R_{g0} and R_{h0} are the numerator of Eqs. (17) and (18), respectively when the di-block PA has a straight chain structure. It turns out from Figure 5(a) that there is no disagreement in the average energy obtained from different simulations for $T^* \sim 0.05$. However the discrepancy of the average energy between Simulation I and others becomes large with lowering the temperature. It is considered that the di-block PA in Simulation I must be trapped into a

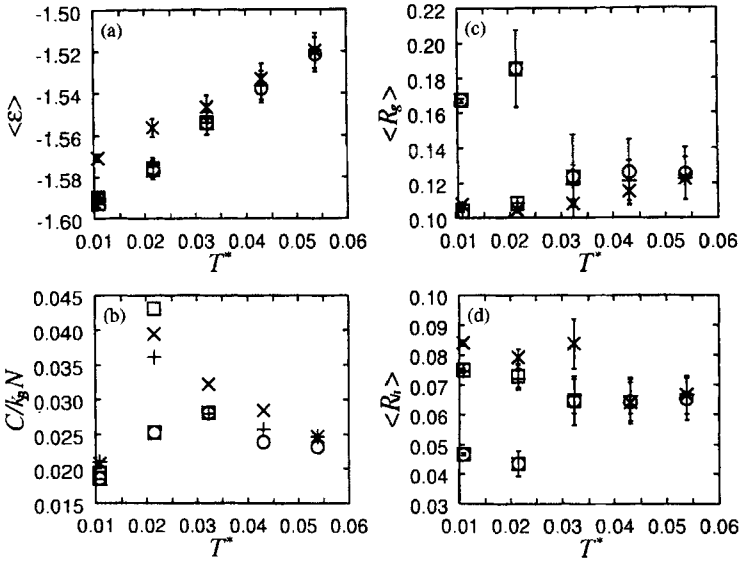

FIGURE 5 The temperature dependence of (a): potential energy, (b): specific heat, (c): $\langle R_g \rangle$ and (d): $\langle R_h \rangle$. "×", "+", "○" and "□" indicate the results of Simulation I, II, III and IV, respectively. The significance of Simulations I, II, III and IV is mentioned in the text. $\langle \varepsilon \rangle = (\langle E \rangle)/N)/(e^2/r_0)$, where $\langle E \rangle$ is the statistical average of the potential energy (see Eq. (1)).

local minimum state or a glass state because of a quench process in Simulation I. Figure 6 shows the distribution of distance between all monomers' pairs ($P(r_{ij})$) obtained by (a): simulation IV-5 and (b): Simulation I at $T^* \sim 0.01$. In these figures the sharp peak of dashed and dotted lines at $r_{ij} = 1$ almost comes from $P(r_{ii+1})$, but the peak of solid line at $r_{ij} = 1$ is a result of Coulomb attraction between unlike monomers' pairs. In Figure 6(a) there are several clear peaks in $P(r_{ij})$ and the distribution of positive monomers around positive monomers (dashed line) and the distribution of negative monomers around negative monomers (dotted line) are almost the same as naturally being expected. Although in Figure 6(b) peaks in $P(r_{ij})$ are not so clear as in Figure 6(a) except for the peak at $r_{ij} = 1$, it turns out that the distribution of positive monomers around positive monomer (dashed line) and the distribution of negative monomers around negative monomer (dotted line) are slightly different. If the di-block PA is in a certain equilibrium state, dashed line and dotted line should be the same. Thus it is considered that the state of Figure 6(b) is not thermodynamically equilibrium, but a glassy (non-equilibrium) state. Also it turns out that $P(r_{ij})$s' obtained by Simulation I at $T^* \sim 0.02$, 0.03 and 0.04 are different from those obtained by either simulations II-2, 3 and 4 or simulations III-2, 3 and 4. Hence the conventional

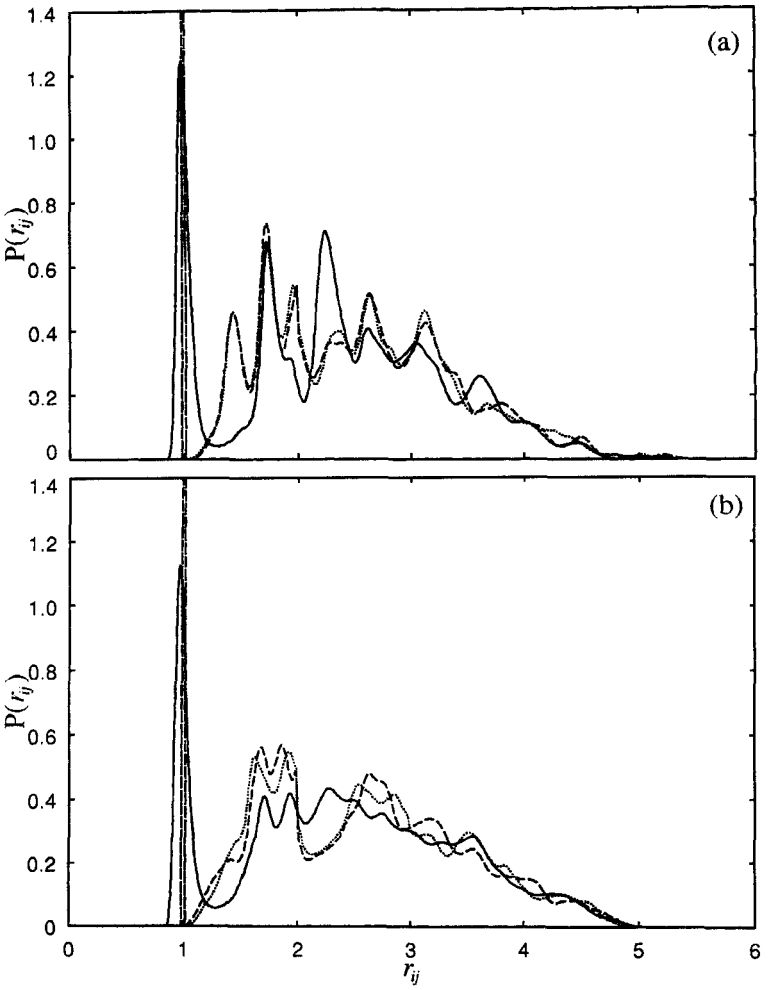

FIGURE 6 The distribution of monomer pair distances obtained by (a): Simulation IV-5, and (b): Simulation I at $T^* \sim 0.01$. The solid line is the distribution of unlikely charged monomer pairs, the dashed line the distribution of positively charged monomers around a positively charged monomer and dotted line the distribution of negatively charged monomers around a negatively charged monomer. The unit of horizontal axis is r_0.

canonical MD simulation at temperatures below $T^* \sim 0.05$ results only in locally minimum states or glassy states. Figure 5(b) shows the temperature dependence of the specific heat. The temperature dependence of the specific heat obtained by Simulation I is similar to that of Simulation II and both have a peak around $T^* \sim 0.02$. On the other hand, no such a peak is found in Simulation III. The specific heat increases monotonically in the first 3

processes of Simulation IV, the same processes as Simulation III, while it behaves differently in the last 2 processes of Simulation IV. When the temperature being gradually lowered from $T^* \sim 0.03$ to $T^* \sim 0.01$, it indicates a peak around $T^* \sim 0.02$ (simulation IV-4) around which Simulations I and II also show a peak. Hence a hysteresis of the specific heat is remarkable in Simulation IV. The temperature dependence of gyration radius ($\langle R_g \rangle$) and hairpin parameter ($\langle R_h \rangle$) are shown in Figures 5(c) and (d), respectively. In these figures the results of Simulation I differs slightly from the results of Simulation II. $\langle R_g \rangle$ and $\langle R_h \rangle$ obtained by the simulations III-1 and 2 are quite different either from those of Simulations I, II or simulations IV-4 and 5. The initial state of simulation III-1 which was taken from the MMD simulation at $T^* \sim 0.108$ as a low energy structure is shown in Figure 7(a). This is a double helical structure. Such structure has

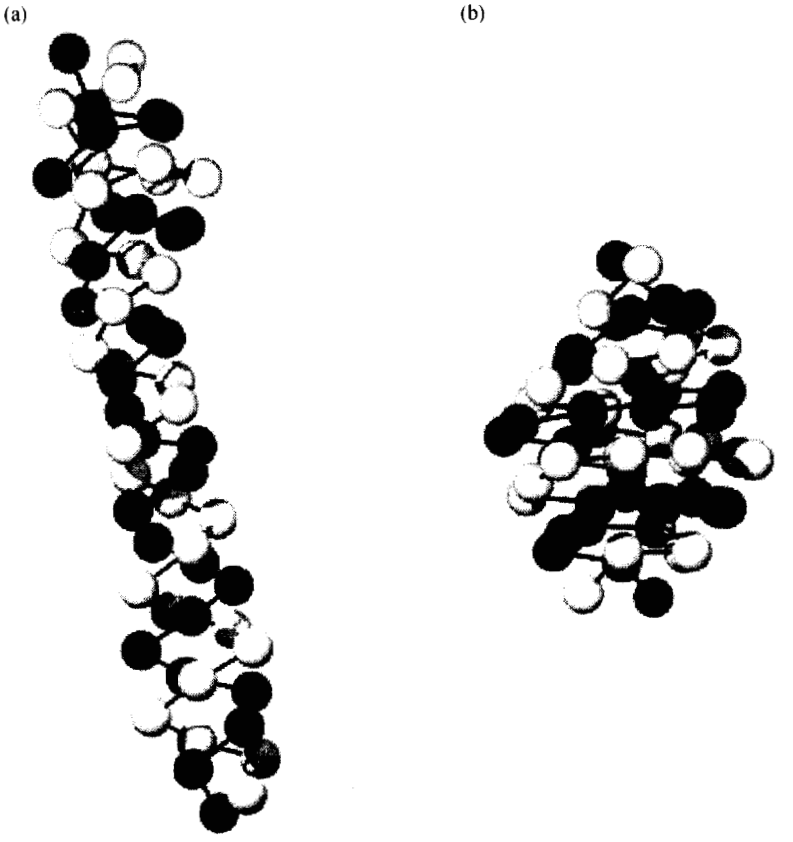

FIGURE 7 The snapshot of di-block PA. (a): the lowest energy conformation found in the MMD simulation. (b): a low energy conformation found in the simulation IV-5.

been retained during the simulations III-1 and 2 so that $\langle R_g \rangle$ becomes large and $\langle R_h \rangle$ becomes small. When the temperature is raised up to $T^* \sim 0.03$ (simulation III-3), this helical structure is lost and the di-block PA falls into a spherical structure. During the simulation IV-4 and 5 the di-block PA has always taken a spherical structure and never returned into the structure shown in Figure 7(a). $\langle R_g \rangle$ and $\langle R_h \rangle$ of simulations IV-4 and 5 become almost the same to those of Simulation II. The snapshot of the lowest energy conformation of simulation IV-5 is shown in Figure 7(b), which has a spherically helical structure. The lowest energy conformation of simulation II-5 also has such a structure. The present system can take at least these two helical structures in low temperature region. The spherical structure is more stable than the stretched double helical structure. $\langle R_g \rangle$ obtained by Simulation I at $T^* \sim 0.01$ is similar to that of simulations II-5 and IV-5. However the conformation at the lowest energy state does not have a helical structure. During the quenching process (Simulation II and simulations IV-4 and 5), the specific heat has a peak around $T^* \sim 0.02$, a slight change of $\langle R_g \rangle$ is obtained between $T^* \sim 0.02$ and $T^* \sim 0.03$ and $\langle R_h \rangle$ increases with lowering temperature below $T^* \sim 0.03$. Moreover $P(r_{ij})$ obtained simulation II-3 (Fig. 8) is significantly different from $P(r_{ij})$ obtained by simulation II-5 (Fig. 6(a)). This suggests that the first order-like phase transition takes place

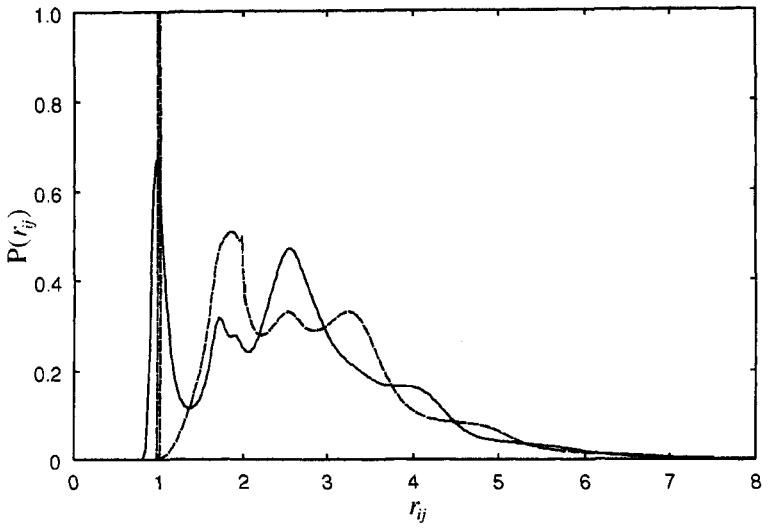

FIGURE 8 The distribution of monomer pair distances at $T^* \sim 0.03$ (simulation II-3). The solid line is the distribution of unlikely charged monomer pairs, the dashed line the distribution of positively charged monomers around a positively charged monomer and dotted line the distribution of negatively charged monomers around a negatively charged monomer. The unit of horizontal axis is r_0.

around $T^* \sim 0.02$, though it may be improper to use 'phase' for the present system which contains only one di-block PA with a finite length. It turns out that the peaks of $P(r_{ij})$ in Figure 6(a) correspond to $r_{ij} = 1, \sqrt{2}, \sqrt{3}, 2, \sqrt{5}$ and $\sqrt{7}$, exhibiting a crystalline like structure with small $\langle R_g \rangle$ and large $\langle R_h \rangle$ at $T^* \sim 0.01$.

5. CONCLUSION

We have carried out MD simulations for a di-block PA. The MMD simulation results are in good agreement with the results of conventional canonical MD over the temperature region where the canonical MD simulation results are reliable. For lower temperatures the MMD simulation is expected to give us more reliable results in which the phase (structural) transition appears.

Previous work on the di-block PA [4–8] has mainly been concerned with the dependence of gyration radius on the temperature and the charge invariance. In the present work we have shown two low energy states of double helical structures at temperature $T^* \sim 0.01$, though this does not rule out the possibility of other structures. We have obtained a spherical helix from Simulation II and the transition from the stretched helical structure to the spherical helix. However we have not found the reverse transition. This suggests that the spherical helix is more stable than the stretched helix. It is necessary to calculate the free energy as a function of gyration radius and/or hairpin parameter to determine the most stable structure. To this end it is highly desired to apply the MMD method in low temperature region.

Acknowledgments

This study was supported by the Original Industrial Technology R&D Promotion Program from the New Energy and Industrial Technology Development Organization (NEDO) of Japan.

References

[1] Anfinsen, C. B. (1973). "Principles that Govern the Folding of Protein Chains", *Science*, **181**, 223.
[2] Levinthal, C. (1968). "Are there Pathways for Protein Folding?", *J. Chim. Phys.*, **65**, 44.
[3] Minor, D. L. Jr. and Kim, P. S. (1996). "Context-dependent secondary structure formation of a designed protein sequence", *Nature*, **380**, 730.
[4] Higgs, P. G. and Joanny, J. F. (1991). "Theory of polyampholyte solutions", *J. Chem. Phys.*, **94**, 1543.
[5] Kantor, Y., Li, H. and Kardar, M. (1992). "Conformations of Polyampholytes", *Phys. Rev. Lett.*, **69**, 61.

[6] Kantor, Y., Kardar, M. and Li, H. (1994). "Statistical mechanics of polyampholytes", *Phys. Rev. E*, **49**, 1383.
[7] Tanaka, M., Grosberg, A. Y., Pande, V. S. and Tanaka, T. (1997). "Molecular dynamics study of the structure organization in a strongly coupled chain of charged particles", *Phys. Rev. E*, **56**, 5798.
[8] Victor, J. M. and Imbert, J. B. (1993). "Collapse of an Alternating Polyampholyte: Evidence for Tricriticality in 2 and 3 Dimensions", *Europhys. Lett.*, **24**, 189.
[9] Berg, B. A. and Neuhaus, T. (1991). "Multicanonical algorithms for first order phase transitions", *Phys. Lett. B*, **267**, 249.
[10] Nakajima, N., Nakamura, H. and Kidera, A. (1997). "Multicanonical Ensemble Generated by Molecular Dynamics Simulation for Enhanced Conformational Sampling of Peptides", *J. Chem. Phys.*, **101**, 817.
[11] Hoover, W. G., Ladd, A. J. C. and Moran, B. (1982). "High-Strain-Rate Plastic Flow Studied *via* Nonequilibrium Molecular Dynamics", *Phys. Rev. Lett.*, **48**, 1818.
[12] Evans, D. J. (1983). "Computer "experiment" for nonlinear thermodynamics of Couette flow", *J. Chem. Phys.*, **78**, 3297.
[13] Yoneya, M., Berendsen, H. J. C. and Hirasawa, K. (1994). "A Non-iterative Matrix Method for Constraint Molecular Dynamics Simulations", *Mol. Sim.*, **13**, 395.
[14] Yoneya, M. and Ouchi, T. (1995). "Molecular Dynamics Simulations on Shared-memory Multiple Processor Computers", *Mol. Sim.*, **15**, 273.
[15] Slusher, J. T. and Cummings, P. T. (1996). "Non-iterative Constraint Dynamics Using Velocity-explicit Verlet Methods", *Mol. Sim.*, **18**, 213.
[16] Swope, W. C., Andersen, H. C., Berens, P. H. and Wilson, K. R. (1982). "A computer simulation method for the calculation of equilibrium constants for the formation of physical clusters of molecules: Application to small water clusters", *J. Chem. Phys.*, **76**, 637.